Azimuthal directions of equatorial noise propagation determined using 10 years of data from the Cluster spacecraft

F. Nemec, O. Santolík, J. S. Pickett, Z. Hrbackova, Nicole Cornilleau-Wehrlin

JOURNAL OF GEOPHYSICAL RESEARCH: SPACE PHYSICS, VOL. 118, 7160–7169, doi:10.1002/2013JA019373, 2013

Azimuthal directions of equatorial noise propagation determined using 10 years of data from the Cluster spacecraft

F. Němec,[1] O. Santolík,[1,2] J. S. Pickett,[3] Z. Hrbáčková,[1,2] and N. Cornilleau-Wehrlin[4,5]

Received 26 August 2013; revised 22 October 2013; accepted 31 October 2013; published 21 November 2013.

[1] Equatorial noise (EN) emissions are electromagnetic waves at frequencies between the proton cyclotron frequency and the lower hybrid frequency routinely observed within a few degrees of the geomagnetic equator at radial distances from about 2 to 6 R_E. They propagate in the extraordinary (fast magnetosonic) mode nearly perpendicularly to the ambient magnetic field. We conduct a systematic analysis of azimuthal directions of wave propagation, using all available Cluster data from 2001 to 2010. Altogether, combined measurements of the Wide-Band Data and Spectrum Analyzer of the Spatio-Temporal Analysis of Field Fluctuations instruments allowed us to determine azimuthal angle of wave propagation for more than 100 EN events. It is found that the observed propagation pattern is mostly related to the plasmapause location. While principally isotropic azimuthal directions of EN propagation were detected inside the plasmasphere, wave propagation in the plasma trough was predominantly found directed to the West or East, perpendicular to the radial direction. The observed propagation pattern can be explained using a simple propagation analysis, assuming that the emissions are generated close to the plasmapause.

Citation: Němec, F., O. Santolík, J. S. Pickett, Z. Hrbáčková, and N. Cornilleau-Wehrlin (2013), Azimuthal directions of equatorial noise propagation determined using 10 years of data from the Cluster spacecraft, *J. Geophys. Res. Space Physics*, *118*, 7160–7169, doi:10.1002/2013JA019373.

1. Introduction

[2] Intense electromagnetic waves observed in the equatorial region of the inner magnetosphere were reported for the first time by *Russell et al.* [1970], who called them "equatorial noise" (EN). OGO 3 magnetic field data revealed that the emissions were located in the outer plasmasphere at frequencies between about twice the proton cyclotron frequency (Ω_{H+}) and half the lower hybrid frequency. They were confined within about 2° of the geomagnetic equator, with the magnetic field fluctuations nearly linearly polarized along the ambient magnetic field. Taking into account theoretical properties of electromagnetic waves in cold plasma [*Stix*, 1992], this corresponds to the propagation nearly perpendicular to the ambient magnetic field. In the low-frequency domain, the appropriate wave mode is the fast magnetosonic mode. Thus, EN emissions are often called "fast magnetosonic waves." They can be also linked to the whistler mode at higher frequencies. Observations of EN recorded by the IMP 6 and the Hawkeye 1 satellites at radial distances from about 2 to 5 R_E were analyzed by *Gurnett* [1976]. He showed that EN consists of a complex superposition of many harmonically spaced lines, with several distinctly different frequency spacings often evident in the same spectrum. Further observations showed that equatorial noise can occur at radial distances between 2 and 7 R_E and at latitudes within 10° from the geomagnetic equator [*Laakso et al.*, 1990; *Kasahara et al.*, 1994].

[3] The frequency structure of the EN events appears to be characteristic of the proton cyclotron frequency in the source region [*Gurnett*, 1976; *Perraut et al.*, 1982; *Kasahara et al.*, 1994]. Energetic protons with ring-like distribution functions at a pitch angle of 90° observed in association with the waves [*Perraut et al.*, 1982; *Boardsen et al.*, 1992] are believed to drive the growth [*Perraut et al.*, 1982; *McClements and Dendy*, 1993; *McClements et al.*, 1994; *Horne et al.*, 2000; *Liu et al.*, 2011]. *Horne et al.* [2000] found that the growth is possible at frequencies $\omega > 30\Omega_{H+}$ for proton ring distribution functions with ring velocities v_R exceeding the Alfvén speed ($v_R > v_A$) and at frequencies $\omega < 30\Omega_{H+}$ for proton ring distribution functions with ring velocities $v_R > 2v_A$. The waves were not expected to grow inside the plasmasphere, but the authors have shown that the waves generated just outside the plasmapause can propagate

[1]Faculty of Mathematics and Physics, Charles University in Prague, Prague, Czech Republic.
[2]Institute of Atmospheric Physics, Academy of Sciences of the Czech Republic, Prague, Czech Republic.
[3]Department of Physics and Astronomy, University of Iowa, Iowa City, Iowa, USA.
[4]Laboratoire de Physique des Plasmas, Ecole Polytechnique, CNRS, Palaiseau, France.
[5]LESIA, Observatoire de Meudon, Meudon, France.

Corresponding author: F. Němec, Faculty of Mathematics and Physics, Charles University in Prague, V Holešovičkách 2, 18000 Prague, Czech Republic. (frantisek.nemec@gmail.com)

2169-9380/13/10.1002/2013JA019373

to $L \approx 2$ with very little attenuation, suggesting that waves observed well inside the plasmasphere could originate from a source region just outside the plasmasphere.

[4] *Santolík et al.* [2002] reported high-resolution multipoint observations of equatorial noise performed by the Spectrum Analyzer of the Spatio-Temporal Analysis of Field Fluctuations (STAFF-SA) and the Wide-Band Data (WBD) instruments on board the Cluster spacecraft. They used theoretical polarization properties of EN emissions to present observational evidence that the waves propagate with a significant radial component. The waves can thus propagate from a distant region located at radial distances where ion cyclotron frequencies match the observed fine structure of spectral lines. A systematic analysis of EN emissions observed by the Cluster spacecraft revealed that the occurrence rate at radial distances between 3.9 and 5 R_E is about 60% [*Santolík et al.*, 2004]. These results were further extended by *Němec et al.* [2005, 2006], who demonstrated that EN events occasionally observed farther out from the magnetic equator are probably caused by problems with determining the true magnetic equator. They also showed that the local plasma number density at the spacecraft location can be estimated using the cold plasma theory from the observed B/E ratio. Equatorial noise was found to be the most intense natural emission in the given interval of frequencies and latitudes, indicating that it could play a nonnegligible role in the dynamics of the inner magnetosphere. The effects of EN interaction with radiation belt electrons have been recently discussed by several authors [*Horne et al.*, 2007; *Shprits et al.*, 2013; *Mourenas et al.*, 2013], showing an increased interest in this electromagnetic emission.

[5] Ray tracing studies of EN emissions were performed by *Kasahara et al.* [1994] and *Xiao et al.* [2012]. It was shown that the emissions can propagate Westward or Eastward, perpendicular to the radial direction, especially near the plasmapause. Moreover, they can propagate inward and outward, crossing the plasmapause boundary. A simple analytical ray tracing approximation, based on the assumption of exactly perpendicular propagation, and the equatorial medium symmetrical about the Earth's magnetic dipole axis, was recently presented by *Chen and Thorne* [2012].

[6] We present an analysis of azimuthal angles of EN propagation observed by the Cluster spacecraft at radial distances of about $4R_E$, i.e., close to the plasmapause. All available Cluster data from 2001 to 2010 are used, and the obtained results are discussed in terms of the propagation pattern inside/outside the plasmasphere. The obtained results have important implications for the possible location of the source region. Section 2 describes the data set used in the study. Section 3 introduces the data processing. The obtained results are presented in section 4 and discussed in section 5. Finally, section 6 contains a brief summary.

2. Data Set

[7] Electromagnetic wave data measured by the Cluster spacecraft during the first 10 years of operations (2001–2010) have been used. There are four Cluster satellites which move in a close formation along an elliptical orbit. The apogee was about 119,000 km, and the perigee was about 24,000 km during the first years of the mission (the spacecraft orbit slightly changed over the duration of the mission). The spacecraft are spinning at one rotation every 4 s, with the rotation axis about perpendicular to the ecliptic. Two different wave instruments were used, as they well complement each other for the purpose of this study.

[8] The Wide-Band Data (WBD) Plasma Wave investigation instruments provide high-resolution waveform measurements of AC electric and magnetic fields [*Gurnett et al.*, 1997]. In the continuous baseband measurement mode relevant for our study, the data are band-pass filtered in the frequency range of about 70 Hz–9.5 kHz and measured with the sampling frequency of 27,443 Hz. The WBD instruments cycle between obtaining waveforms of one electric field component measured in the spin plane of the spacecraft for approximately 42 s and waveforms of one magnetic field component for approximately 10 s. However, as we will show later on, only the WBD electric field measurements are relevant for our study. This means that each interval of about 42 s of continuous data is effectively followed by about a 10 s long data gap. An additional complication is that due to the high telemetry rate and the need for ground stations to receive the WBD data directly from the spacecraft, the WBD instruments are active only during specifically selected time intervals (approximately 4% of the orbit).

[9] Lower resolution multicomponent measurements are performed continuously by the Spectrum Analyzer of the Spatio-Temporal Analysis of Field Fluctuations (STAFF) experiments, STAFF-SA [*Cornilleau-Wehrlin et al.*, 1997, 2003]. STAFF-SA instruments use three orthogonal magnetic field components and two electric field components in the spin plane of the spacecraft to calculate the elements of the 5×5 complex spectral matrices. The analysis is performed on board, and it is limited to 27 logarithmically spaced frequency channels between 8 Hz and 4 kHz. One spectral matrix per frequency channel and time interval is obtained. This permits to retrieve information about power spectral densities, mutual phases, and coherence, which can be used to determine detailed wave polarization and propagation properties [see, e.g., *Santolík et al.*, 2003, and the references therein].

[10] The present study uses a list of EN events manually identified in the STAFF-SA data obtained during all Cluster equatorial passes from 2001 to 2010 [*Hrbáčková et al.*, 2012]. Altogether, the list contains 2465 EN events. However, due to the specificity of the equatorial noise wave mode, the WBD electric field measurements are needed for the intended analysis of azimuthal directions of wave propagation. Only the EN events measured during the times when the WBD instruments were active are thus used. This limits the number of analyzed events to 226.

3. Data Processing

[11] An example of an EN event measured by the STAFF-SA instrument on board Cluster 4 on 23 April 2002 is shown in Figure 1. The plotted data were acquired during a 15 min long time interval between 0230:00 UT and 0245:00 UT. The first panel shows the frequency-time spectrogram of power spectral density of magnetic field fluctuations. The second, third, and fourth panels show frequency-time plots of wave properties determined using the singular value decomposition (SVD) method [*Santolík et al.*, 2003]. These

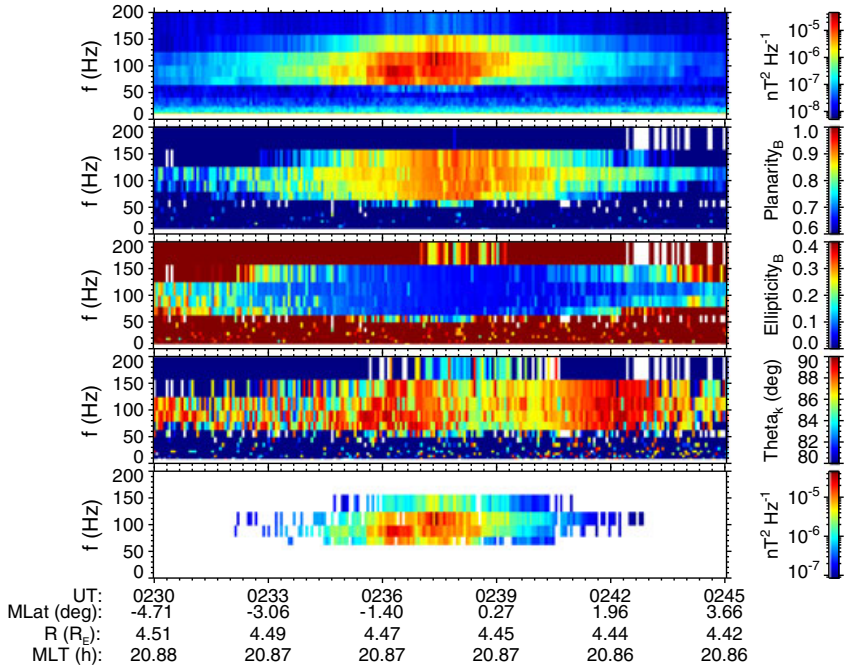

Figure 1. Example of an EN event, along with a detailed wave analysis using the SVD method (see text). The data were measured on 23 April 2002 by the STAFF-SA instrument on Cluster 4. The individual panels correspond to (from the top) frequency-time spectrogram of power spectral density of magnetic field fluctuations, frequency-time plot of the planarity of magnetic field fluctuations, frequency-time plot of the ellipticity of magnetic field fluctuations, and frequency-time plot of the polar angle of the wave vector direction. The last panel is the same as the first panel (i.e., it shows the frequency-time spectrogram of power spectral density of magnetic field fluctuations), but this time only the frequency-time subintervals that fulfill the conditions set for EN emissions (planarity > 0.8, ellipticity < 0.2, $\theta_k > 85°$) are plotted.

are (from the top) planarity of magnetic field fluctuations, ellipticity of magnetic field fluctuations, and polar angle of the wave vector direction with respect to the ambient magnetic field. In the first part of the data processing, these propagation parameters are used to select the frequency-time subintervals which contain the EN emissions.

[12] The planarity of magnetic field fluctuations may range from 0 to 1. It is used to express how well an assumption of a single plane wave is fulfilled, i.e., how well the magnetic field fluctuations are confined to a single plane. The values of planarity close to 1 correspond to a situation when the polarization ellipsoid degenerates into a single plane. The values of planarity close to 0 correspond to a situation when the polarization ellipsoid degenerates into a sphere, i.e., no preferred direction exists. Magnetic field fluctuations corresponding to EN emissions are expected to be nearly linearly polarized along the ambient magnetic field. The corresponding values of planarity are thus expected to be close to 1. A histogram of experimentally determined values of planarity corresponding to EN emissions has been shown by *Santolík et al.* [2004]. According to their results (see their Figure 3b), a reasonable minimum threshold value of planarity for an emission to qualify as EN is about 0.8. We have adopted this value for the purpose of the present paper.

[13] The values of ellipticity of magnetic field fluctuations, which is defined as a ratio of the minor to the major polarization axes, may range from 0 to 1. The values of ellipticity equal to 0 correspond to a linear polarization. The values of ellipticity equal to 1 correspond to a circular polarization. Magnetic field fluctuations corresponding to EN emissions are nearly linearly polarized. A histogram of experimentally determined values of ellipticity corresponding to EN emissions has been shown by *Santolík et al.* [2004]. According to their results (see their Figure 2b), a reasonable upper bound value of ellipticity required for an emission to qualify as EN is about 0.2 or less. We have adopted this value as a maximum threshold for the purpose of the present paper.

[14] EN emissions propagate nearly perpendicularly to the ambient magnetic field, so that the polar angle of the wave vector direction with respect to the ambient magnetic field should be close to 90°. For the purpose of the present paper, we adopt a threshold value for the polar angle of the wave vector direction of 85°. Note, however, that the three analyzed wave parameters (planarity, ellipticity, and wave normal angle) are not independent; they rather are quite tightly related. Namely, according to the theory of electromagnetic waves in cold plasmas, a wave propagating at wave normal angles close to 90° in the extraordinary mode has magnetic field fluctuations nearly linearly polarized along the ambient magnetic field. This means that the ellipticity of magnetic field fluctuations is close to 0. It also implies that the planarity of magnetic field fluctuations should be large, even if several EN emissions propagating at the same time in different (azimuthal) directions are assumed.

Nevertheless, as the natural measured data contain some amount of noise, it is still useful to set several (albeit not independent) conditions, all of which must be fulfilled for an emission to qualify as EN.

[15] We have employed the following three conditions to identify frequency-time subintervals corresponding to the EN emissions: (i) the planarity larger than 0.8, (ii) the ellipticity lower than 0.2, and (iii) wave normal angle larger than 85°. As the values of these parameters are evaluated in each frequency-time subinterval of the STAFF-SA data depicted in Figure 1, we obtain binary information of whether a given frequency-time subinterval can be considered as EN or not. The result of this simple threshold identification is shown in the last panel of Figure 1. It shows the same values as the first panel, i.e., the power spectral densities of magnetic field fluctuations, but only for the frequency-time subintervals that fulfill all the three conditions. It can be seen that the procedure works reasonably well. Although some of the frequency-time intervals at the edges of the event were excluded, the core of the event remained.

[16] However, in order to analyze the azimuthal directions of wave propagation, it is not desirable to identify the individual frequency-time subintervals fulfilling the EN criteria. We rather have to identify the whole time intervals corresponding to EN events, i.e., to determine, for each frequency band of the STAFF-SA instrument, the times when a given EN event starts and ends. Principally, the aim is—after the thresholds for the planarity, the ellipticity, and the wave normal angle are applied—to find the longest continuous data interval. This is separately done for each of the eight frequency bands of the STAFF-SA instrument between 70 Hz (lowest frequency detectable by the WBD electric field measurements) and 400 Hz (upper estimate of the lower hybrid frequency at the spacecraft location). The results of the procedure applied to the example event from Figure 1 are shown in Figure 2. The individual panels correspond to the individual frequency bands of the STAFF-SA instrument where EN was observed. As there may be some minor gaps in EN frequency-time subintervals determined using the threshold identification procedure (as it can be seen in the bottom panel of Figure 1), we allow for gaps of up 20 s long (i.e., five consecutive frequency-time subintervals, taking into account the 4 s time resolution of the spectral matrices). This value was determined as an optimal value using a test set of events. It enables to fill in the sometimes occurring gaps but prevents us from false identifications. The result of this procedure applied to the example event is shown in Figure 2 by the blue vertical dashed lines. It can be seen that the identification works reasonably well in the sense that the identified boundaries are rather close to what a human would naturally mark as the beginning and the end of the event. We note that it would be wrong to use simply the first and last valid frequency-time subinterval, as this would in some cases lead to an identification of unreasonably long time intervals of EN.

[17] Applying the above described procedure for identification of EN time intervals to all 226 EN events for which the WBD data are at least partially available results in a total of 123 EN events at frequencies larger than 70 Hz that fulfilled the selection criteria. This corresponds to a total of 361 frequency-time intervals of EN. Note that the number of EN frequency-time intervals is a factor of about 3 larger than the number of EN events. The reason is that the time intervals are identified separately for each frequency band of the STAFF-SA instrument, and an EN event can span over several frequency bands.

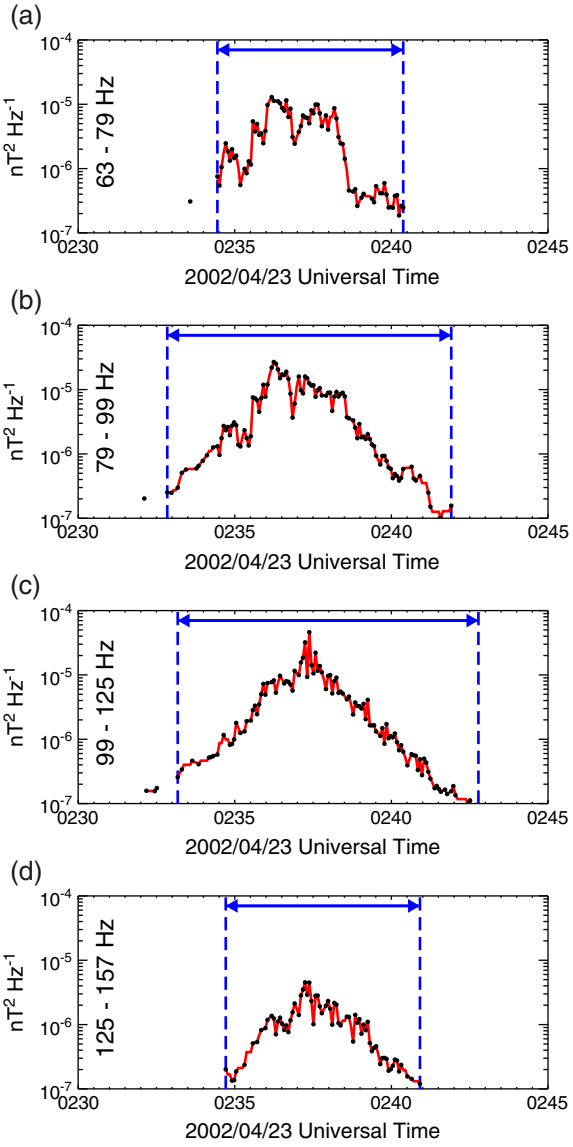

Figure 2. Power spectral density of magnetic field fluctuations as a function of time. The plotted time interval is exactly the same as in Figure 1. The individual panels correspond to the individual frequency bands of the STAFF-SA instrument where EN was observed. The appropriate frequency bounds are given on the left side of the panels. The time intervals corresponding to EN emissions identified by the automatic procedure (see text) are marked by the blue vertical dashed lines.

[18] Having identified the frequency-time intervals of EN with the WBD data coverage, we can proceed to perform the intended analysis of the azimuthal directions of the wave propagation. A conventional wave normal analysis cannot be straightforwardly applied to EN due to the linear polarization of magnetic field fluctuations of EN emissions: it is based on the fact that magnetic field fluctuations are,

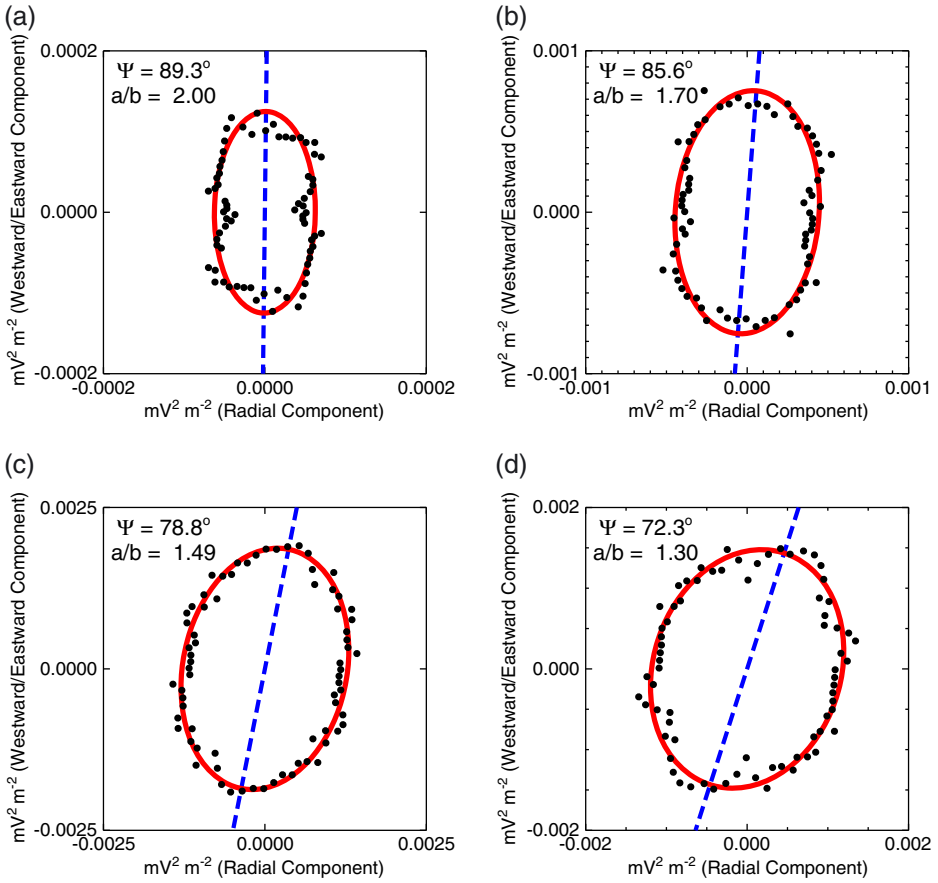

Figure 3. Polar plots of the median wave power measured by the WBD instruments during the time intervals of EN occurrence shown in Figure 2. Each of the four plots corresponds to a different frequency range (the same as in Figure 2). The red curves show the best-fit ellipses, which are used as an approximation of the observed angular dependence of the detected wave power. The directions of the major axes (i.e., the wave vector directions) are shown by the blue dashed lines. The appropriate azimuthal angles, along with the ratios of major to minor axes, are given in the individual plots.

in general, polarized perpendicularly to the wave vector direction, so that determining the wave vector direction is in fact equivalent to determining the polarization plane. The direction normal to the polarization plane is then the direction of the wave vector. Unfortunately, as the magnetic field fluctuations corresponding to EN are linearly polarized, the polarization plane degenerates into a line (parallel to the ambient magnetic field). The infinite number of perpendicular directions then does not allow for the determination of a wave normal. The magnetic field fluctuations are therefore insufficient for the determination of the wave vector direction, and the electric field measurements have to be used.

[19] The idea is the same as it was successfully applied by *Santolík et al.* [2002] in a case study of EN propagation. We use the fact that the electric field fluctuations corresponding to EN emissions are elliptically polarized in the equatorial plane, with the major polarization axis oriented in the direction of the wave vector. Moreover, the Cluster spacecraft rotate with the frequency of about 0.25 Hz, i.e., with the frequency significantly lower than the period of EN emissions. At the times when the Cluster spacecraft cross the geomagnetic equator, the electric field antenna is oriented approximately in the polarization plane of EN electric field fluctuations. The electric field intensity observed by a single antenna on board Cluster should therefore exhibit a modulation of the wave intensity with a period of about 4 s. The orientation of the antenna at the times when the maximum intensity is detected then corresponds to the direction of the wave vector (with an ambiguity of $\pm 180°$). We correct for a small deviation of the antenna direction from the equatorial plane (i.e., the theoretical polarization plane of the electric field fluctuations) by dividing the waveform values by the cosine of this angular deviation, which is known from the spacecraft attitude data.

[20] The analysis is done—for a given EN event—in several frequency bands, which are defined to correspond to the frequency bands of the STAFF-SA instruments. The electric field waveform measured by the WBD instrument is digitally band-pass filtered in the required frequency band. The square of the filtered electric field waveform then corresponds to the wave power observed by the electric field antenna in a given frequency range. This wave power exhibits two principal modulations. There is the aforementioned modulation due to the spacecraft rotation. Moreover, there is a modulation corresponding to the wave

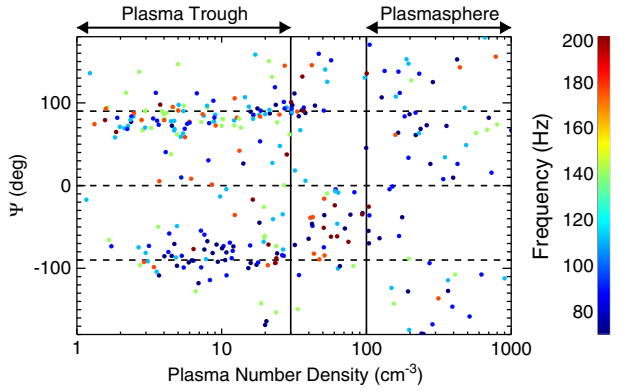

Figure 4. Azimuthal angles of the wave propagation as a function of the local plasma number density determined from the B/E ratio. Central frequencies of the appropriate frequency bands of the STAFF-SA instrument are color coded using the scale on the right. Low-density region (plasma trough) and high-density region (plasmasphere) with qualitatively different propagation patterns are marked.

oscillation, i.e., a modulation with a period corresponding to the wave frequency. In order to remove the latter modulation, we calculate moving averages of the wave power over a time duration corresponding to the wave period. In this way, the wave power as a function of the antenna orientation is obtained. Note that this calculation benefits from the fact that the wave period is generally much lower than the period of the Cluster spacecraft rotation. Also note that the time intervals used for the calculation of the moving averages are—due to computational requirements—shifted by the number of waveform samples corresponding to one half of the wave period. This has principally no negative effect on the obtained results (except of lower azimuthal resolution of mean wave power) but significantly speeds up the calculation.

[21] As a single EN event lasts usually rather long compared to the Cluster rotation period, there are typically many Cluster rotations during a single EN event. This results in many values of detected wave power in a given azimuthal direction. Azimuthal bins 5° wide have been used for the purpose. This value represents a good compromise between the requirement of a fine azimuthal resolution and a reasonable number of data points falling in a given bin. A median value of the wave power in a given direction is therefore used for further analysis, which allows for a convenient filtering out of extremely large/low values of the wave power. Moreover, as there is an ambiguity of ±180°, the geometry is symmetric and only azimuthal angle values from –90° to +90° are considered.

[22] An example of the dependencies obtained for the four frequency ranges of the STAFF-SA instrument where the EN event occurred in the example case from Figure 1 is shown in Figure 3. Each of the four plots corresponds to a different frequency range. These are the same as in Figure 2. Polar plots of the median electric field spectral power measured by the WBD instrument during the time intervals corresponding to the EN occurrence shown in Figure 2 are plotted by the black points. Although the calculation itself is performed only for azimuthal angles from –90° to +90°, the median wave power is plotted for azimuthal angles from –180° to +180°, using the fact that the wave power at an angle α is equal to the wave power at an angle $\alpha + 180°$.

[23] The red curves in Figure 3 show best-fit ellipses, which are used as an approximation of the observed angular dependence of the wave power. Most importantly, the directions of their major axes are shown by the blue dashed lines. The azimuthal angles of major polarization axes, along with the ratio of major to minor polarization axes, are given in the individual panels. These are the principal results corresponding to the wave propagation in a given frequency range. Namely, the azimuthal angles of the major axes correspond to the wave vector directions, and the ratios of major to minor axes provide information about how well the preferred directions of the wave propagation are determined. These results are used in the remainder of the paper.

[24] The ambiguity of ±180° in the azimuthal angle of wave propagation cannot be solved by using the WBD data, as the phase relations between electric and magnetic field fluctuations are needed. These are provided by the STAFF-SA instrument. The STAFF-SA measurements could be therefore used to determine the directions of EN propagation on their own. However, EN emissions have rather special polarization properties. Moreover, the emissions propagate in many directions simultaneously, and a unique wave propagation direction generally does not exist. Consequently, the determination of the azimuthal angle of wave propagation using exclusively STAFF-SA data was found to be very imprecise, if not impossible. The WBD data and the analysis described above are therefore used to determine the azimuthal angle of wave propagation, and the STAFF-SA data are used only to resolve the ambiguity problem. This is done by assuming the two possible propagation directions determined from the WBD data and evaluating which of them is more consistent with the B/E phase relations measured by the STAFF-SA instrument. Namely, we use the fact that—assuming a single plane wave propagating exactly perpendicular to the ambient magnetic field—the phase of magnetic field fluctuations (B_z, linearly polarized along the ambient magnetic field) is 90° behind the phase of the electric field fluctuations in the direction of the wave vector. This allows us to solve the ambiguity problem by comparing the sign of the imaginary component of the spectral matrix element calculated from B_z and one electric field component with the sign theoretically calculated for a given antenna orientation. Only the electric field antenna more aligned with the wave vector direction was used for the calculation.

4. Results

[25] We have determined the azimuthal directions of EN propagation for all available EN events. The obtained results are presented in Figure 4, which shows the calculated azimuthal angles as a function of the plasma number density at the spacecraft location. The plasma number density has been determined from the measured ratio of magnetic to electric power spectral densities using the cold plasma theory dispersion relation [*Němec et al.*, 2006]. The plasma number densities obtained in this way are in an overall agreement with plasma number densities determined from the spacecraft potential [see Němec

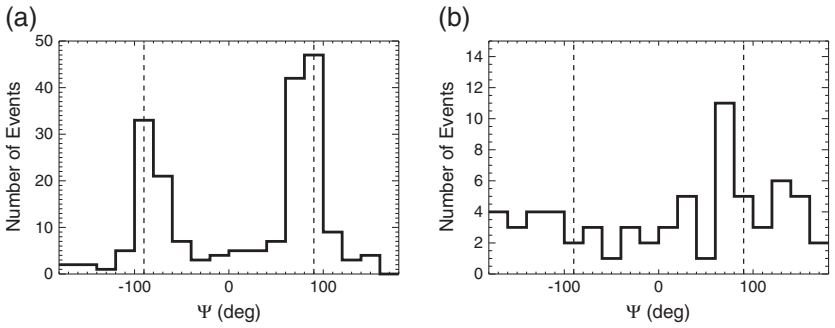

Figure 5. Histograms of the calculated values of the azimuthal angles of the wave propagation in the (a) plasma trough and (b) plasmasphere. Azimuthal angles of ±90° corresponding to the propagation in the eastward/westward direction are shown by the dashed vertical lines.

et al., 2006, Figures 6 and 7], and they can be readily derived directly from EN observations. Among the possible parameters that we have analyzed, most importantly the radial distance of the spacecraft, it was the plasma number density at the spacecraft location that best organized the data.

[26] Two regions with different propagation properties can be identified in Figure 4. In the left-hand side of the figure, i.e., in the low-density region called, for the purpose of this paper, (and approximately corresponding to) the plasma trough, the azimuthal angles of the wave propagation are found to be mostly close to ±90°. This corresponds to propagation in a direction perpendicular to the radial direction. The value of the azimuthal angle equal to 90° means an eastward propagation, and the value of azimuthal angle equal to –90° means a westward propagation. In contrast, in the right-hand side of the figure, i.e., in the high density region called, for the purpose of this paper, (and approximately corresponding to) the plasmasphere, the wave propagation can be principally in any direction, with none of them being significantly preferred. The two density regions are marked at the top of the figure. Note that there is a transition region with medium plasma number densities, classified neither as the plasma trough nor as the plasmasphere, where the observed azimuthal angles are somewhere in between the two above described patterns. The central frequencies of the appropriate frequency bands of the STAFF-SA instruments are color coded using the scale on the right. Note that the low number of events occurring in the plasmasphere is due to the fact that the EN events observed in the plasmasphere have on average lower frequencies than the EN events observed in the plasma trough, so that many of them occur at frequencies below 70 Hz. A possible explanation of this phenomenon will be discussed in section 5.

[27] Histograms of the calculated values of the azimuthal angles of the wave vector directions in the plasma trough and in the plasmasphere are shown in Figures 5a and 5b, respectively. The overall impression from Figure 4 concerning the preferred directions of wave propagation is confirmed. Moreover, some more subtle details can be seen. Absolute values of the azimuthal angles of the wave propagation in the plasma trough are close to 90°, but in most cases slightly lower. This corresponds to a situation of nearly azimuthal propagation, but with a small radial component oriented away from the Earth. All azimuthal angles of wave propagation have been observed in the plasmasphere. Note, however, that the accuracy of the azimuthal distribution in Figure 5b is somewhat limited by the low number of events occurring in the plasmasphere.

[28] The ratios of major to minor axes of the best-fit ellipses as a function of the estimated local plasma number density are shown in Figure 6. Following the format of Figure 4, the central frequencies of the appropriate frequency bands of the STAFF-SA instruments are color coded using the scale on the right. The two density regions, plasma trough and plasmasphere, are also distinguished. Moreover, the median values of the major to minor axes ratios in these density regions are marked by the thick horizontal lines. It can be seen that the ratios are generally larger in the plasma trough than in the plasmasphere. This indicates that the directions of propagation in the plasma trough are typically well defined. However, the wave propagation in the plasmasphere can be rather complicated, with waves propagating in several directions at the same time.

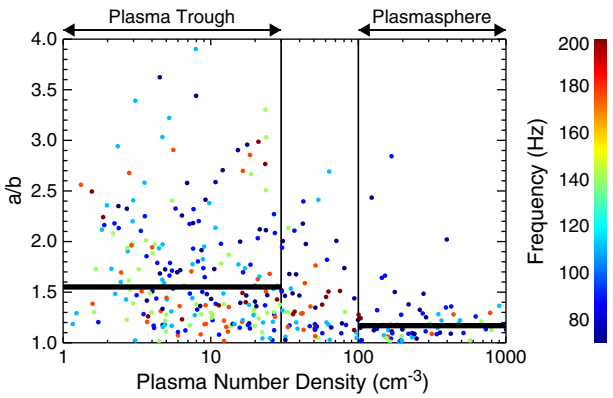

Figure 6. Ratios of major to minor axes of the best-fit as a function of the local plasma number density. Following Figure 4, the central frequencies of the appropriate frequency bands of the STAFF-SA instruments are color coded, and the plasma trough and the plasmasphere regions are marked. Median values in these two density regions are shown by the thick horizontal lines.

5. Discussion

[29] The assumption of a single plane wave is generally invalid in the case of EN [*Santolík et al.*, 2002]; i.e., there are several waves at a given frequency propagating in different directions. However, our procedure based on the modulation of the detected wave power caused by the Cluster rotation works well even in this situation of a more complicated propagation. It still enables us to determine the preferred direction of the wave propagation, and moreover, it allows us to at least roughly estimate the beaming pattern.

[30] The crucial parameter related to the amount of the wave energy propagating in the preferred direction of the wave propagation is the ratio of major to minor axes of the best-fit ellipse. Assuming that the ellipticity of electric field fluctuations corresponding to EN emissions is close to 0 [*Santolík et al.*, 2002], the azimuthal dependence of the observed wave power corresponding to a single propagating plane wave should be $W(\psi) = [E(\psi_0)\cos(\psi - \psi_0)]^2$, where $W(\psi)$ is the wave power detected in the azimuthal direction ψ, ψ_0 is the direction of the wave propagation, and $E(\psi_0)$ is the wave power in this direction. This means that there should be no wave power detected in the direction perpendicular to the wave propagation in this idealized case. Nevertheless, in the real situation, this is not the case, and a significant amount of the wave power is detected in the direction perpendicular to the preferred propagation direction. Empirically, the azimuthal dependence of the observed wave power approximately follows an ellipse. The ratio of the major to minor axes of this ellipse expresses how well the wave power is beamed in the preferred direction of propagation. The larger the ratio is, the more wave power is directed in the preferred direction of propagation, i.e., the closer the situation is to a single plane wave. In the extreme case of no preferred direction of propagation, the ratio is equal to 1, and the wave power propagates equally in all directions.

[31] The obtained results concerning the wave propagation show that EN emissions propagate principally in all directions inside the plasmasphere (although westward/eastward propagation seems to be slightly preferred). The ratios of major to minor axes of best-fit ellipses are generally rather low, indicating again a complicated propagation pattern with waves propagating in many different directions. The propagation outside the plasmasphere is rather different. The vast majority of EN events in the plasma trough propagates either in the westward or in the eastward direction (none of them appears to be preferred). Moreover, the ratios of major to minor axes of best-fit ellipses are larger than those in the plasmasphere, in agreement with the situation of better determined directions of preferred wave propagation. The plasmapause boundary seems to have a crucial importance for the propagation of EN emissions. Hereinafter, we shall discuss why this should be the case, and what are the implications of the observed propagation pattern for the source region of EN emissions.

[32] The ray tracing of individual propagating EN waves is needed to understand the overall propagation scheme. However, due to the symmetry of the situation, it is not necessary to employ the full numerical ray tracing code, but a simplified description of the ray paths is possible [*Chen and Thorne*, 2012]. Assuming the propagation exactly perpendicular to the ambient magnetic field, and an idealized situation axially symmetric about the axis of the Earth's magnetic dipole, it can be shown that $Q = nL\sin\psi$ is conserved along the ray path, where n is the refractive index, L is the McIlwain L-parameter, and ψ is the azimuthal angle of the wave propagation. Note that in this idealized situation, the group velocity and the phase wave velocity have the same direction, and the propagating wave stays in the equatorial plane. The refractive index of the extraordinary mode wave, which can be conveniently calculated using the Stix parameters [*Stix*, 1992], is approximately proportional to the ratio between the electron plasma frequency and the electron cyclotron frequency. This suggests that the plasmapause boundary should have a significant impact on the propagation of EN emissions, as it is the boundary where a rapid decrease of the refractive index is expected. Cluster perigee equatorial passes are especially interesting in this point of view. They take place at radial distances of about 4 R_E, i.e., at about the mean plasmapause distance, occurring sometimes in the plasmasphere and sometimes in the plasma trough.

[33] *Chen and Thorne* [2012] performed an extensive theoretical analysis of EN propagation using the aforementioned simplifying assumptions. We use their method of calculation, with only minor modifications in the representation of the results, in order to demonstrate more clearly the point that we want to make. The principal aim is to analyze the propagation of EN emissions through the plasmapause. A model plasma density profile used in the calculations is shown in Figure 7a. The plasmapause location was set to $L = 4$, and the model plasma number density dependence of *Denton et al.* [2004] has been used both in the plasmasphere and in the plasma trough. Electron densities in the narrow region around the plasmapause were calculated in order to provide a smooth transition between the plasmasphere and the plasma trough. However, the propagation of EN emissions through the plamapause is—at least qualitatively—nearly independent of the exact shape of the plasma number density profile used. The main point is that while the plasma number density decreases only slowly with radial distance in the plasmasphere and in the plasma trough, it suddenly drops at the plasmapause.

[34] This sudden drop causes, in turn, a sudden drop of the refractive index. This is demonstrated in Figure 7b, which shows the color-coded value of the refractive index as a function of the frequency and the radial distance. The values of the refractive index were calculated using the cold plasma theory, assuming a dipole magnetic field model, the plasma number density profile from Figure 7a, and the propagation exactly perpendicular to the ambient magnetic field. Moreover, we have assumed a pure hydrogen plasma, with no heavier ions present. Helium and oxygen ions which are expected to be present during the disturbed periods would increase the values of the refractive index by a factor approximately equal to the square root of the ratio of average ion to proton masses. We note in this regard that 15 out of the 123 analyzed events occurred during Kp > 4 periods. However, the qualitative result of the refractive index drop at the plasmapause remains unchanged.

[35] The white area in Figure 7b corresponds to the frequency-radial distance interval where the electromagnetic emissions in the extraordinary mode cannot propagate, i.e., to the frequencies larger than the lower hybrid frequency. The lower hybrid frequency is shown by the upper

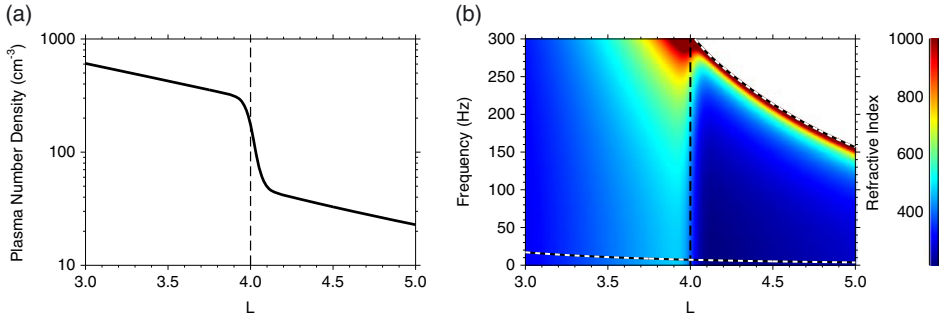

Figure 7. (a) Model plasma number density profile used for refractive index calculations. The dashed vertical line at $L = 4$ shows the position of the plasmapause. (b) Refractive index calculated using the cold plasma theory for the propagation exactly perpendicular to the ambient magnetic field as a function of the L-shell and the frequency. A dipole magnetic field model and the plasma number density profile from Figure 7a were assumed. The lower hybrid frequency is shown by the upper dashed white-black line. The lower dashed white-black line shows the proton cyclotron frequency. The white area corresponds to the part of the plot where the electromagnetic emissions in the extraordinary mode cannot propagate.

dashed white-black line. The lower dashed white-black line shows the proton cyclotron frequency. It can be seen that going from the Earth toward larger radial distances (larger L values), the refractive index gradually increases until the plasmapause is reached. At the plasmapause, there is a sudden jump-like decrease of the refractive index. In the plasma trough, a slow gradual increase of the refractive index is expected. As for the frequency dependence of the refractive index, it can be seen that qualitatively the same behavior of the refractive index at the plasmapause is observed over a large range of frequencies. However, it is noticeable that at high frequencies close to the lower hybrid frequency, the sudden decrease of the refractive index at the plasmapause gets smaller and eventually disappears.

[36] Having obtained the radial dependence of the refractive index, we can evaluate how the azimuthal angle of EN propagation would evolve. Let us assume an emission inside the plasmasphere propagating perpendicularly to the ambient magnetic field at an azimuthal angle ψ and reaching the plasmapause. Since $Q = nL \sin\psi$ is conserved during the propagation, and there is a sudden decrease of the refractive index n at the plasmapause, the sine of the azimuthal angle of the wave propagation must increase accordingly. As the sine of an angle cannot get larger than 1, two principally different situations can occur.

[37] For the original azimuthal angle of the wave propagation larger than some critical value ψ_c ($\psi > \psi_c$), the wave gets reflected by the plasmapause, and it propagates back to lower radial distances. As demonstrated by *Chen and Thorne* [2012], such a wave may reflect at lower radial distances due to gradually decreasing values of the refractive index (see Figure 7b at $L < 4$) and become effectively trapped. The waves with original azimuthal angles $\psi < \psi_c$ do not get reflected at the plasmapause, and they are merely bent when propagating through it. As the quantity Q must be conserved during the process, the azimuthal angle of the wave propagation increases. The relation can be further simplified by assuming that the L-value does not change across the boundary. In such a case, a simple Snell's law is obtained; i.e., the sine of the azimuthal angle of the wave propagation increases by a factor equal to the ratio of refractive indices inside and outside the boundary. We believe that this bending/reflection of EN emissions at the plasmapause provides an explanation of the observed directions of the wave propagation.

[38] Taking into account a source that radiates isotropically in all azimuthal angles, this necessarily assumes the wave generation inside the plasmasphere, rather close to the plasmapause. This is further supported by the fact that the directions of propagation of EN emissions observed in the plasma trough often have a small radial component oriented away from the Earth. The location of the generation region of EN emissions close to the outer boundary of the plasmasphere might seem to be in agreement with theoretical calculations by *Horne et al.* [2000], who showed that the growth of the emissions is possible when the proton ring distribution with the ring velocity exceeding the Alfvén speed is present. This would suggest that the regions with low Alfvén speed might be preferred source regions of EN emissions, and the radial profile of the Alfvén speed has a local minimum at the outer boundary of the plasmasphere. However, *Horne et al.* [2000] predicted principally no wave growth inside the plasmasphere, because of the Bessel function weighting term in their equation (2) and the ring velocity $v_R >> v_A$.

[39] If the wave generation took place outside the plasmasphere, the waves would have to be generated preferentially at azimuthal angles close to $\psi = \pm 90°$. We do not see any reason why the growth rate of the waves should be larger at these azimuthal angles. However, it is possible to imagine that a radially limited source region with a significant azimuthal extent could result in a longer amplification path in the azimuthal direction and therefore waves being generated preferentially in $\psi = \pm 90°$ direction. Assuming that the generation would take place just outside the plasmasphere, this alternative scenario would also explain why the directions of propagation of EN emissions observed in the plasma trough typically have a small radial component oriented away from the Earth. We are unable to unambiguously distinguish which of the suggested scenarios is correct, i.e., if the generation region is located just inside or just outside the plasmasphere. Nevertheless, the generation region is located close to the plasmapause in both cases.

[40] EN emissions observed in the plasmasphere have often frequencies lower than 70 Hz, while higher-frequency EN emissions are observed primarily in the plasma trough. We believe that this is consistent with the generation region located close to the plasmapause. Assuming the same harmonic numbers of the generated emissions, EN emissions with higher frequencies are generated when the magnetic field magnitude at the generation region is larger than normal, i.e., at the times when the generation region moves closer to the Earth. This, in turn, corresponds to the periods when the plasmapause is at radial distances lower than usual. Taking into account that the Cluster perigee equatorial passes in the analyzed time interval mostly take place at radial distances of about $4R_E$, i.e., at about the mean location of the plasmapause, the situation of the compressed plasmasphere results in the Cluster equatorial passes in the plasma trough. The higher frequencies of EN emissions observed in the plasma trough are therefore likely to be a sampling effect. Alternatively, a source not necessarily moving closer to the Earth along with the plasmapause during disturbed periods, but generating emissions at higher harmonic numbers, could also explain why higher-frequency EN emissions are observed in the plasma trough.

6. Conclusions

[41] Azimuthal directions of propagation of EN emissions have been analyzed using all available Cluster data from 2001 to 2010. Altogether, combined WBD and STAFF-SA measurements allowed us to determine the azimuthal angle of the wave propagation in more than 100 EN events. We have shown that the propagation pattern is well organized according to the local plasma number density at the spacecraft location, being principally different in the low density region (plasma trough) than in the high density region (plasmasphere). While effectively all directions of EN propagation are detected inside the plasmasphere (with only a weak preference for westward/eastward propagation), the wave propagation in the plasma trough is found to be in either westward or eastward direction (with neither of them significantly preferred). These results demonstrate that the plasmapause has crucial implications for the propagation of EN emissions. The observed propagation pattern can be explained using a simple propagation analysis, assuming that EN emissions are generated close to the plasmapause.

[42] **Acknowledgments.** We would like to thank the Cluster Active Archive and all the involved personnel. A part of the Cluster WBD data set for this study has been received at the Panska Ves Observatory of the Institute of Atmospheric Physics ASCR and we would like to thank its personnel. This work was supported by GACR grants P209/12/P658 and P205/10/2279 and by GAUK grant 678212. This work was supported at Iowa by NASA Goddard Space Flight Canter grant NNX11AB38G.

[43] Robert Lysak thanks the reviewers for their assistance in evaluating this paper.

References

Boardsen, S. A., D. L. Gallagher, D. A. Gurnett, W. K. Peterson, and J. L. Green (1992), Funnel-shaped, low-frequency equatorial waves, *J. Geophys. Res.*, *97*, 14,967–14,976.

Chen, L., and R. M. Thorne (2012), Perpendicular propagation of magnetosonic waves, *Geophys. Res. Lett.*, *39*, L14102, doi:10.1029/2012GL052485.

Cornilleau-Wehrlin, N., et al. (1997), The Cluster spatio-temporal analysis of field fluctuations (STAFF) experiment, *Space Sci. Rev.*, *79*, 107–136.

Cornilleau-Wehrlin, N., et al. (2003), First results obtained by the Cluster STAFF experiment, *Ann. Geophys.*, *21*, 437–456, doi:10.5194/angeo-21-437-2003.

Denton, R. E., J. D. Manietti, J. Goldstein, S. L. Young, and R. R. Anderson (2004), Electron density in the magnetosphere, *J. Geophys. Res.*, *109*, A09215, doi:10.1029/2003JA010245.

Gurnett, D. A. (1976), Plasma wave interactions with energetic ions near the magnetic equator, *J. Geophys. Res.*, *81*, 2765–2770.

Gurnett, D. A., R. L. Huff, and D. L. Kirchner (1997), The wide-band plasma wave investigation, *Space Sci. Rev.*, *79*, 195–208.

Horne, R. B., G. V. Wheeler, and H. S. C. K. Alleyne (2000), Proton and electron heating by radially propagating fast magnetosonic waves, *J. Geophys. Res.*, *105*(A12), 27,597–27,610.

Horne, R. B., R. M. Thorne, S. A. Glauert, N. P. Meredith, D. Pokhotelov, and O. Santolik (2007), Electron acceleration in the Van Allen radiation belts by fast magnetosonic waves, *J. Geophys. Res.*, *34*, L17107, doi:10.1029/2007GL030267.

Hrbáčková, Z., O. Santolík, F. Němec, and N. Cornilleau-Wehrlin (2012), Occurrence rate of magnetosonic equatorial noise emissions as a function of the McIlwain's parameter, paper presented at EGU General Assembly Conference Abstracts, Vienna, Austria.

Kasahara, Y., H. Kenmochi, and I. Kimura (1994), Propagation characteristics of the ELF emissions observed by the satellite Akebono in the equatorial plane, *Radio Sci.*, *29*, 751–767.

Laakso, H., H. Junginger, A. Roux, R. Schmidt, and C. de Villedary (1990), Magnetosonic waves above f_{cH+} at geostationary orbit: GEOS 2 results, *J. Geophys. Res.*, *95*, 10,609–10,621.

Liu, K., S. P. Gary, and D. Winske (2011), Excitation of magnetosonic waves in the terrestrial magnetosphere: Particle-in-cell simulations, *J. Geophys. Res.*, *116*, A07212, doi:10.1029/2010JA016372.

McClements, K. G., and R. O. Dendy (1993), Ion cyclotron harmonic wave generation by ring protons in space plasmas, *J. Geophys. Res.*, *98*, 11,689–11,700.

McClements, K. G., R. O. Dendy, and C. N. Lashmore-Davis (1994), A model for the generation of obliquely propagating ULF waves near the magnetic equator, *J. Geophys. Res.*, *99*, 23,685–23,693.

Mourenas, D., A. V. Artemyev, O. V. Agapitov, and V. Karsnoselskikh (2013), Analytical estimates of electron quasi-linear diffusion by fast magnetosonic waves, *J. Geophys. Res. Space Physics*, *118*, 1–17, doi:10.1002/jgra.50349.

Němec, F., O. Santolík, K. Gereová, E. Macúšová, Y. de Conchy, and N. Cornilleau-Wehrlin (2005), Initial results of a survey of equatorial noise emissions observed by the cluster spacecraft, *Planet. Space Sci.*, *53*, 291–298.

Němec, F., O. Santolík, K. Gereová, E. Macúšová, H. Laakso, Y. de Conchy, M. Maksimovic, and N. Cornilleau-Wehrlin (2006), Equatorial noise: Statistical study of its localization and the derived number density, *Adv. Space Res.*, *37*, 610–616.

Perraut, S., A. Roux, P. Robert, R. Gendrin, J. A. Sauvaud, J. M. Bosqued, G. Kremser, and A. Korth (1982), A systematic study of ULF waves above f_{H+} from GEOS 1 and 2 measurements and their relationships with proton ring distributions, *J. Geophys. Res.*, *87*, 6219–6236.

Russell, C. T., R. E. Holzer, and E. J. Smith (1970), OGO 3 observations of ELF noise in the magnetosphere. The nature of the equatorial noise, *J. Geophys. Res.*, *75*(4), 755–768.

Santolík, O., J. S. Pickett, D. A. Gurnett, M. Maksimovic, and N. Cornilleau-Wehrlin (2002), Spatiotemporal variability and propagation of equatorial noise observed by Cluster, *J. Geophys. Res.*, *107*, 1495, doi:10.1029/2001JA009159.

Santolík, O., M. Parrot, and F. Lefeuvre (2003), Singular value decomposition methods for wave propagation analysis, *Radio Sci.*, *38*, 1010, doi:10.1029/2000RS002523.

Santolík, O., F. Němec, K. Gereová, E. Macúšová, Y. de Conchy, and N. Cornilleau-Wehrlin (2004), Systematic analysis of equatorial noise below the lower hybrid frequency, *Ann. Geophys.*, *22*, 2587–2595.

Shprits, Y. Y., A. Runov, and B. Ni (2013), Gyro-resonant scattering of radiation belt electrons during solar minimum by fast magnetosonic waves, *J. Geophys. Res. Space Physics*, *118*, 648–652, doi:10.1002/jgra.50108.

Stix, T. H. (1992), *Waves in Plasmas*, pp. 1–46, Springer-Verlag, New York.

Xiao, F., Q. Zhou, Z. He, and L. Tang (2012), Three-dimensional ray tracing of fast magnetosonic waves, *J. Geophys. Res.*, *117*, A06208, doi:10.1029/2012JA017589.